Asian Journal of Applied Science and Technology (AJAST)
Volume 7, Issue 2, Pages 185-196, April-June 2023

Hydrocarbon Production Induced Faulting in Onshore Fuba Field Niger-Delta, Nigeria, Using 3-D Seismic Time-lapse Data

U. Ochoma*

Department of Physics, Rivers State University, P.M.B 5080, Port Harcourt, Nigeria.
*Email: umaocho@gmail.com**

DOI: https://doi.org/10.38177/ajast.2023.7220

Article Received: 19 April 2023 *Article Accepted: 29 May 2023* *Article Published: 13 June 2023*

ABSTRACT

Hydrocarbon Production Induced Faulting in Onshore Fuba Field Niger Delta, Nigeria, are here presented, using 3D seismic time-lapse data. The FUBA Field lies on latitudes $4^0$50'58''-$4^0$55'19''N and longitudes $6^0$18'41''- $6^0$26'41''E with aerial extent of 840km^2. The base (1997) and the monitor (2009) seismic surveys resulted in a 4D response difference. The Base and Monitor data have a root-mean-square repeatability ratio (RRR) of 0.38 implying a very good repeatability when considering the acquisition, processing and environmental noises. Data processing and interpretation were carried out using Petrel software. Reservoir pressure decline rate of 0.062psi/day resulted in production decline rate of 1192.21bbl/day. Structural interpretation of seismic data reveals a highly faulted field. Two distinct horizons were mapped. Fault and horizon interpretation shows closures that are collapsed crestal structures bounded by two major faults. All the interpreted faults are normal synthetic and antithetic faults which are common in the Niger Delta basin. The depth structure maps reveal anticlinal faults. Reservoirs are found at a shallower depth from 6500 to 7500 ft and at a deeper depth ranging from 11500 to 13000 ft. The variance edge enhanced the faults or sedimentological bodies within the seismic data volume. There are more discontinuities in the difference volume variance edge which implies that there are more cracks in the field of study due to production. The lengths, dips and orientations of the faults and horizons, in the base and monitor stacks, are not equal indicative of faults reactivation that could have resulted from hydrocarbon production. The results of the work can be applied in the hydrocarbon exploitation scheme to minimize the damages associated with production and to ascertain reactivation of faults in the area of study.

Keywords: Seismic, Time-lapse, Anticlinal, Faults, Variance edge, Niger Delta, Nigeria.

1.0. Introduction

The time-lapse seismic method involves using multiple 3D seismic surveys recorded during the field life recorded under same acquisition conditions to determine the changes occurring in the reservoir as a result of hydrocarbon production or injection of water or gas into the reservoir by comparing the repeated datasets (Stammeeijer, and Hatchell, 2014). Time-lapse seismic monitoring of production-induced changes in a reservoir and the surrounding rocks over time has the basic aim of mapping reservoir compartments and subsurface rock deformation, monitoring fluid movement and pore pressure changes, identifying by-passed oil and planning for future production performance, and this has been challenging (Landrø, 2001; Trani, *et al*., 2011; MacBeth, *et al*., 2018). Such integrated geological, geophysical and petroleum engineering methods are needed to create a well-resolved picture of a producing reservoir. Pore pressure depletion creates changes in the stress and strain fields of the rock material both inside and outside the reservoir (Prioul, *et al.*, 2004; Fuck, *et al.* (2011)).

In addition to leakage of hydrocarbons, hazards are associated with wells crossing reactivated faults (Alsos, *et al.* 2002). Reactivated faults can also have close relationships with earthquakes (Zoback, and Zincke, 2002). Many literatures have reported interesting seismic time-lapse studies in the oil prolific area of the Niger Delta Basin, Nigeria. Furthermost, these studies majored on time-lapse feasibility studies and reservoir monitoring and management (Aniwetalu, et al., 2017; Uko, et al., 2018). Moreover, literatures in public domain are very scarce on seismic time-lapse, in Nigeria, with the main objective of determining effect of hydrocarbon production on subsurface structures and faults reactivation (Igwenagu, et al, 2021). Moving beyond uniaxial deformation,

Minkoff, et al, (2004) applied coupled fluid-flow and geomechanical simulations capable of predicting production-induced triaxial (3D) stress evolution and deformation within a compacting reservoir. Herwanger, and Horne, (2007) extended this workflow to predict induced seismic anisotropy and velocity changes due to 3D stress and strain evolution within and outside a reservoir.

This study is taken from Fuba Field, Depobelt, Niger Delta, Nigeria. The ultimate deliverable of this study was hydrocarbon production induced faulting, using 3-D seismic time-lapse data. The major components of this study are: (a) Well Correlation performed in order to determine the continuity of the reservoir sand across the field. (b) Seismic Interpretation which involves differencing of seismic volume, well-to-seismic tie, fault mapping, horizon mapping, time surface generation, depth conversion and seismic attributes generation. This aids in giving more insight into hydrocarbon production induced faulting in onshore Fuba field Niger-Delta, Nigeria, using 3-D seismic time-lapse data.

2.0. Location and Geology of the Study Area

The proposed study area Fuba Field is located in the onshore Niger Delta region. Figure 1 shows the map of the Niger Delta region showing the study area. The Niger Delta lies between latitudes 4° N and 6° N and longitudes 3° E and 9° E (Whiteman, 1982). The Delta ranks as one of the major oil and gas provinces globally, with an estimated ultimate recovery of 40 billion barrels of oil and 40 trillion cubic feet of gas (Adegoke, et al., 2017).

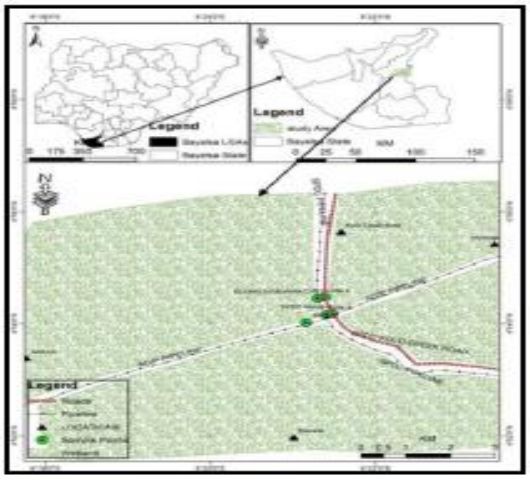

Figure 1. Map of Niger Delta Oilfields showing the location of Fuba Field

The coastal sedimentary basin of Nigeria has been the scene of three depositional cycles (Short, and Stauble, 1967). The first began with a marine incursion in the middle Cretaceous and was terminated by a mild folding phase in Santonian time. The second included the growth of a proto-Niger delta during the Late Cretaceous and ended in a major Paleocene marine transgression. The third cycle, from Eocene to Recent, marked the continuous growth of the main Niger delta. A new threefold lithostratigraphic subdivision is introduced for the Niger delta subsurface, comprising an upper sandy Benin Formation, an intervening unit of alternating sandstone and shale named the Agbada Formation, and a lower shaly Akata Formation. These three units extend across the whole delta and each ranges in age from early Tertiary to Recent. They are related to the present outcrops and environments of deposition. A separate member of the Benin Formation is recognized in the Port Harcourt area. It is Miocene-

Recent in age with a minimum thickness of more than 6,000ft (1829m) and made up of continental sands and sandstones (>90%) with few shale intercalations (Horsfall. et al., 2017). Subsurface structures are described as resulting from movement under the influence of gravity and their distribution is related to growth stages of the delta (Ochoma, et al., 2020). Rollover anticlines in front of growth faults form the main objectives of oil exploration, the hydrocarbons being found in sandstone reservoirs of the Agbada Formation.

3.0. Methodology

3.1. Normalized Root Mean Square (NRMS) Repeatability (RRR) and Differencing of Seismic Volume

Pre-stack time migrated full-offset 3D and 4D stacks were available. The success of time-lapse reservoir monitoring depends on removing the non-repeatable effects such as configurations, seasonal changes, atmospheric temperatures, tides, elastic properties of the overburden, compaction, multiples, and rock heterogeneities (Vedanti, et al., 2009; Varela, et al., 2006). Obstructions, weather patterns, cost constraints, and maritime traffic can also influence the survey orientation. Having considered the above sources of error in repeatability, the acquisition system itself, positioning accuracy, receiver sensitivity/calibration, and source calibration must also be looked into. All these sources of error were handled through normalized root mean square (NRMS) analysis. The NRMS value is simply the RMS amplitude of the difference, normalized by the average of the RMS amplitudes of the baseline data Baseline and monitor data Monitor (Kragh, and Christie, 2002):

$$NRMS = -\frac{2\,rms(Monitor - baseline)}{rms(Monitor) + (Baseline)} \quad (1)$$

$$rms = \sqrt{\frac{\sum x_i^2}{N}} \quad (2)$$

The summation is over N number of all samples x_i (i = 1, 2, · · ·, N) in the time window.

The NRMS value is a measure of non-repeatability. If NRMS = 0, the data are perfectly repeatable. Typical “good” values of NRMS quoted in the literature range from 0.1 to 0.3 [10% to 30% non-repeatability] (Johnston, 2013).

Monitor 4D seismic volume was subtracted from the Base 3D volume, and the differences was interpreted to determine the areas of the field that have been changed during production. Areas of the areas in the field where there have been changes were analyzed and compared to production activity in those areas.

3.2. Well-to-Seismic Ties

Well correlation is the first stage of the pre-interpretation process. The process of well correlation involves lithologic description, picking top and base of sand-bodies, fluid discrimination and then linking these properties from one well to another based on similarity in trends. In between these two lithologies in the subsurface, the gamma ray log is often used. Correlation of reservoir sands was achieved using the top and base of reservoir sands picked. The correlation process was possible based on similarity in the behavior of the gamma ray log the Niger Delta; the predominant lithologies are sands and shales. In order to discriminate shapes. Also, the thickness of the shale bodies overlying and underlying the sand body is considered during Correlation. After defining the lithologies, the resistivity log was used for discriminating the type of fluid occurring within the pores in the rocks.

There are eight basic steps involved in seismic interpretation relevant to this study and they include; Differencing of seismic volume, Well-to-seismic ties, Fault Mapping, Horizon mapping, Time surface generation, Velocity Modelling, Depth Conversion and attributes generation. Well-to-seismic tie is a process that enables the visualization of well information on seismic data. For this process to be achieved, the following are basic requirements; checkshot, sonic log, density log and a wavelet. The sonic log, which is the reciprocal of velocity, was calibrated using the checkshot data. The calibration process is necessary in order to improve the quality of the sonic log because the sonic log is prone to washouts and other wellbore related issues. The results of calibrating the sonic log with the checkshot gives a new log called the calibrated sonic log.

The calibrated sonic log is used along with the density log to generate an acoustic impedance (AI) log. The acoustic impedance log is calculated for each layer of rock. The next step involves generating the reflectivity coefficient (RC) log. The RC is calculated and generated using the AI log. The RC log generated is then convolved with a wavelet to generate a synthetic seismogram which is comparable with the seismic data. The statistical wavelet utilized for convolution is extracted from the seismic data. The synthetic seismogram was generated for every well that had checkshot, density and sonic log. The reflections on the synthetic seismogram were matched with the reflections on seismic data. The mathematical expressions that governs the entire well-to-Seismic tie workflow are presented below;

$$AI = \rho v \qquad (3)$$

$$RC = \frac{\rho_2 v_2 - \rho_1 v_1}{\rho_2 v_2 + \rho_1 v_1} \qquad (4)$$

$$\textit{Synthetic Seismogram} = \frac{\rho_2 v_2 - \rho_1 v_1}{\rho_2 v_2 + \rho_1 v_1} * wavelet \qquad (5)$$

Where ρ= Density, v =Velocity, AI= Acoustic impedance and RC = Reflection coefficient

Faults were identified as discontinuities or breaks in the seismic reflections. Faults were mapped on both inline and cross-line directions. Horizons are continuous lateral reflection events that are truncated by fault lines. The horizon interpretation process was conducted along both inline and crossline direction. At the end of the horizon mapping, a seed grid is generated which serves as an input for time surface generation. Time surfaces were generated using the seed grids gotten from the horizon mapping process. The third order polynomial velocity model was generated and used to depth convert the time surfaces of the reservoirs of interest.

3.3. Variance (Edge Detection) Method

The variance attribute is edge imaging and detection techniques. It is used for imaging discontinuity related to faulting or stratigraphy in seismic data. Variance attribute is proven to help in imaging of channels, fault zones, fractures, unconformities and the major sequence boundaries (Pigott, et al, 2013). In the Petrel software, the variance attribute uses an algorithm that computes the local variance of the seismic data through a multi-trace window with user-defined size. The local variance is computed from horizontal sub-slices for each voxel. A vertical window was used for smoothing the computed variance and the observed amplitude normalized. The variance attribute measures the horizontal continuity of the amplitude that is the amplitude difference of the individual traces from their mean value within a gliding CMP window.

$$\sigma^2 = \frac{1}{n}\sum_{f_i=1}^{n}(x_i + x_m)^2 \qquad (6)$$

Where σ = standard deviation, σ^2 = variance, n = the number of observations, f_i = frequency, x_i = the variable and x_m = mean of x_i

3.4. Dip magnitude and Azimuth

Dip magnitude and azimuth are analogous to strike and dip of sedimentary layers. The dip magnitude is defined as the angle between the steepest direction of a plane and a horizontal plane, where values range from 0 to 90. The dip magnitude attribute computation in Petrel software makes use of the inbuilt formula:

$$\text{True dip} = \tan^{-1}\left(\frac{\tan(\theta_y)}{\tan(\beta_x)}\right) \qquad (7)$$

where θ_y = apparent dip in a direction (y) and β_x = dip azimuth relative to a direction (x).

Dip azimuth is the direction (relative to the north) that plane is dipping, where values range from 0 to 360. The dip azimuth attribute computation in Petrel software makes use of the inbuilt formula:

$$\beta_x = \tan^{-1}\left(\frac{\tan(\theta_x)}{\tan(\theta_y)}\right) \qquad (8)$$

where θ_y = apparent dip in a direction (y), θ_x = apparent dip in a direction (x) and β_x = dip azimuth relative to a direction (x).

Dip magnitude and azimuth are good attributes, not only for showing overall structure folds, but can be used to identify faults with very small displacement.

4.0. Results and Discussion

4.1. Production Data

The production and reservoir pressure reports are presented in Figures 2 and 3. Production decline of 1192.21bbl/day resulted from pressure decline of 95.50bar/year or 0.062psi/year.

4.2. Normalized Root Mean Square (NRMS) Repeatability (RRR) and 4D Response

The NRMS of 0.38 has been achieved, in this study, implying very good repeatability when considering the quality of data and acquisition difference. The seismic time-lapse difference between the base and monitor surveys was successfully extracted. The fact of the difference from the monitor implies the existence of production induced effect and acquisition, environmental and processing noises, hence the 4D or time-lapse response signal.

4.3. Reservoir Identification, Correlation and Well-to-Seismic Ties

The results for lithology and reservoir identification are presented in Figure 4. A total of nine sand bodies (A, B, C, D, E, F, G, H and I) were identified and correlated across all seven wells in the field. Two reservoir sands were selected for the purpose of this study (Reservoirs A and I). The resistivity logs which reveals the presence of

hydrocarbons were used to identify the hydrocarbon bearing sands. On Figure 4, the sands are coloured yellow while shales are grey in colour. The results for well-to-seismic tie conducted on Fuba field using density log, sonic log and checkshot of Well-1 is presented in Figure 5. A statistical wavelet (ISIS time) was used to give a near perfect match between the seismic and synthetic seismogram.

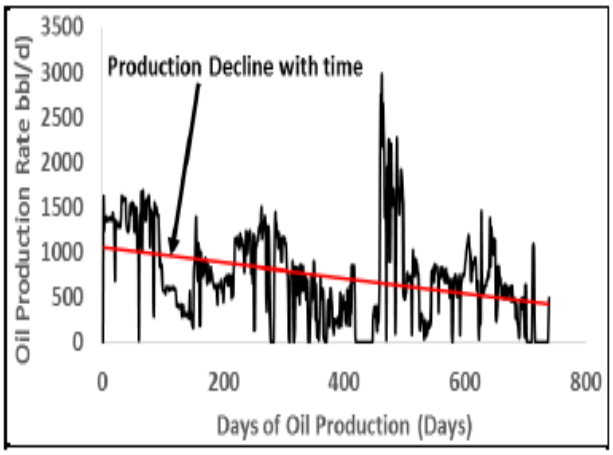

Figure 2. Reservoir Production Rate Versus Days of Oil Production

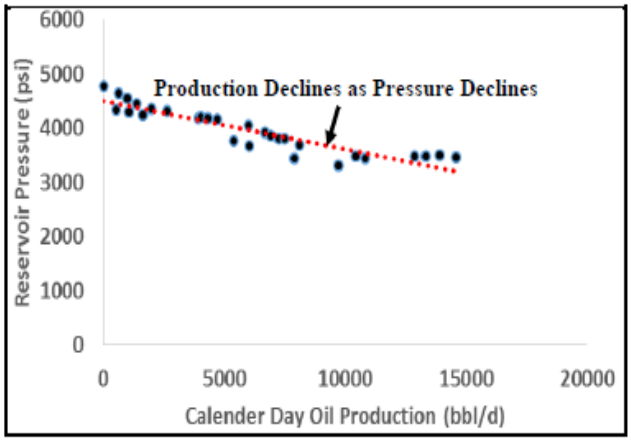

Figure 3. Effect of Reservoir Pressure Decline on Production

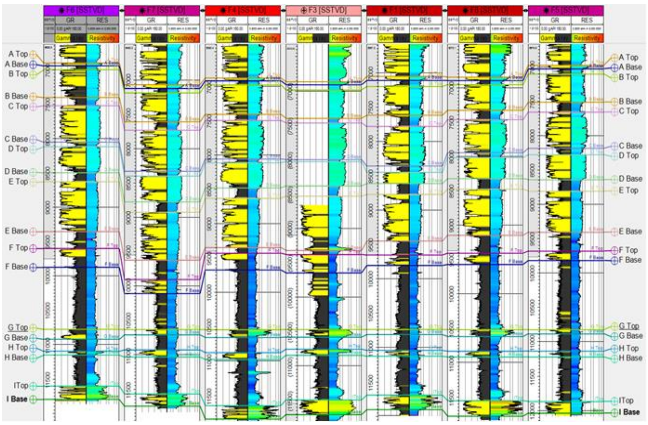

Figure 4. Well section showing reservoir identified and correlated across Fuba Field

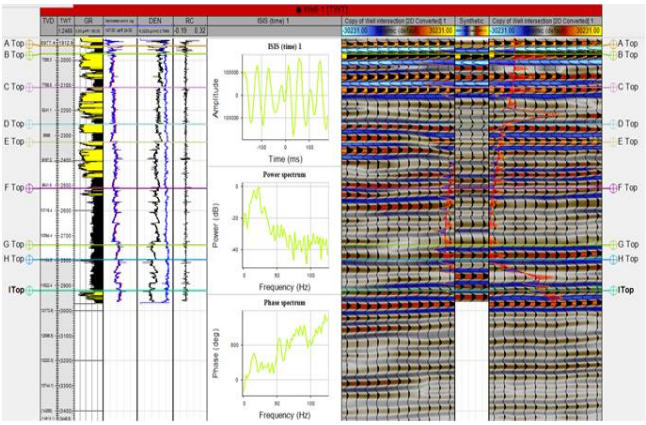

Figure 5. Synthetic seismogram generation and well-to-seismic tie conducted for Fuba Field using Well-1 Checkshot

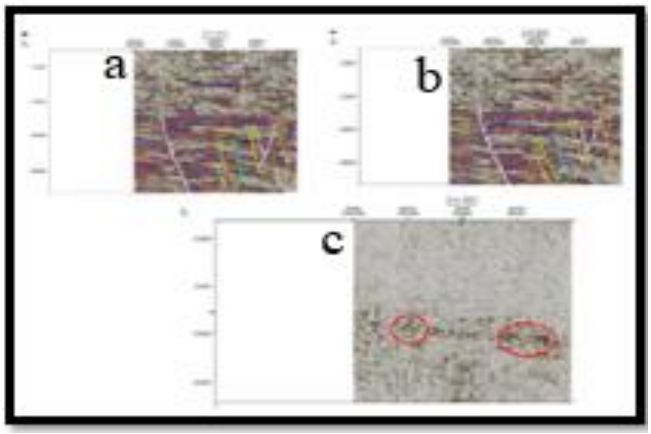

Figure 6. Base, Monitor and Difference Seismic Section for Inline 8590 Interpreted

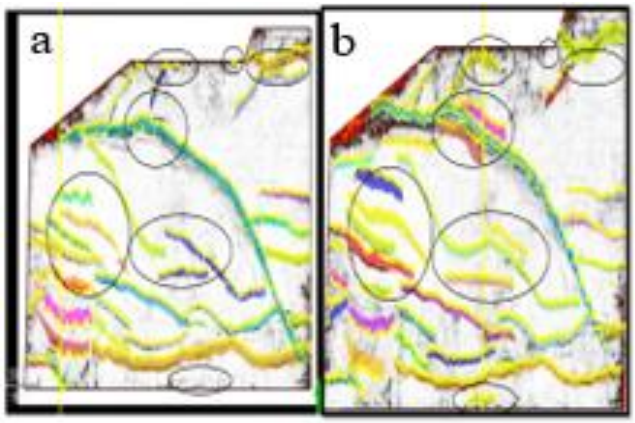

Figure 7. 4D Effect (Diffference) Betweeen Base and Monitor Interpreted Faults Displayed on the Variance Time Slice

Asian Journal of Applied Science and Technology (AJAST)
Volume 7, Issue 2, Pages 185-196, April-June 2023

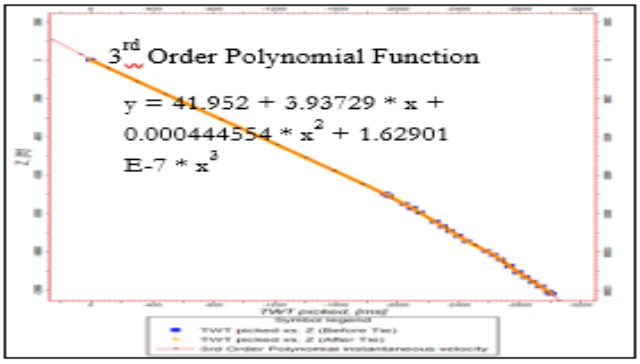

Figure 8. Third Order Polynomial Velocity model for Converting Reservoir Surfaces from Time to Depth

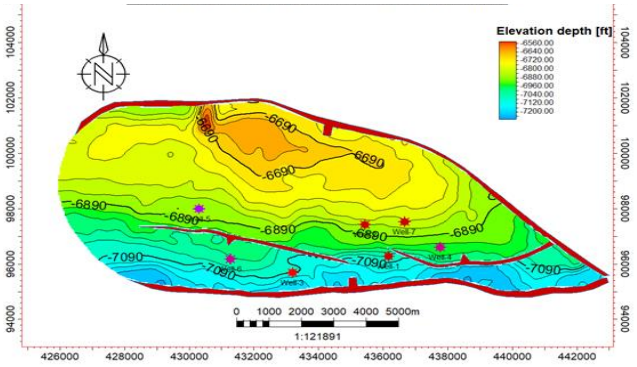

Figure 9. Reservoir Surface for Depth Surface A

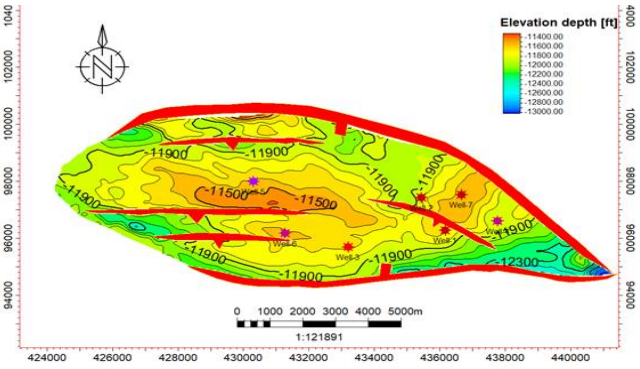

Figure 10. Reservoir Surface for Depth Surface I

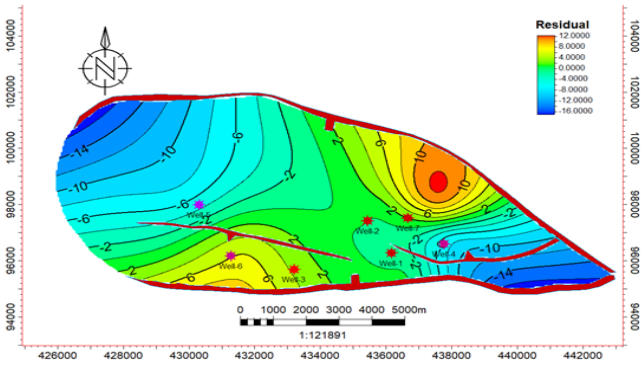

Figure 11. Depth Residual Maps Generated from Surfaces Converted Using the 3rd Order Polynomial Velocity Function for Reservoir A

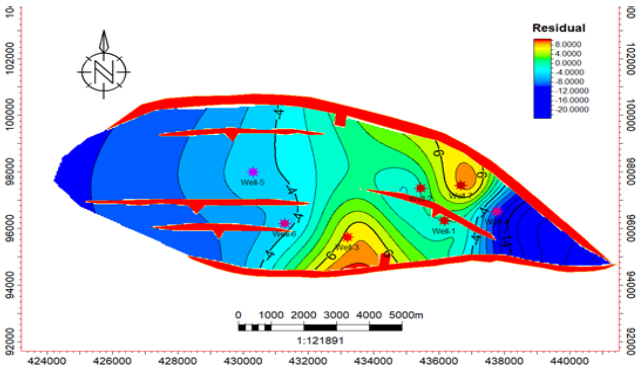

Figure 12. Depth Residual Maps Generated from Surfaces Converted Using the 3rd Order Polynomial Velocity Function for Reservoir I

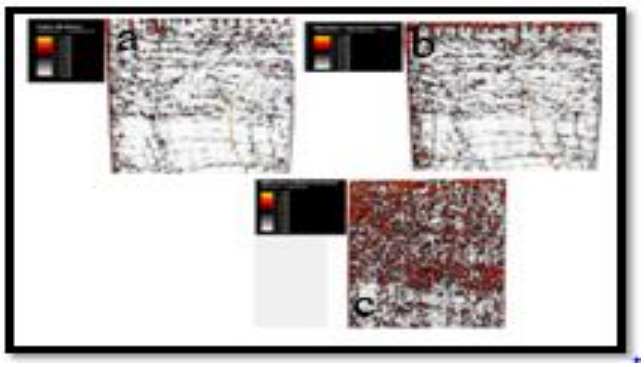

Figure 13. Variance Edge Inline 8515 for Base, Monitor and Difference Volume

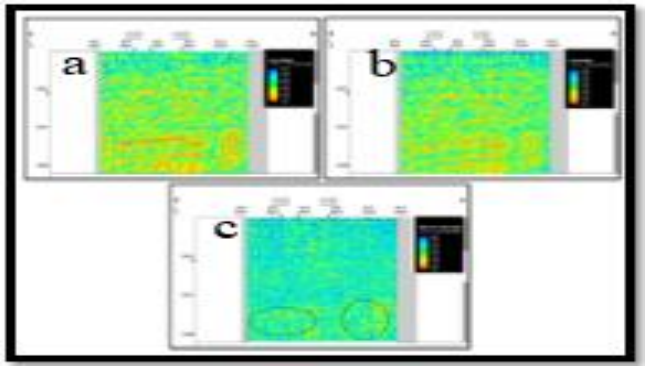

Figure 14. Dip Magnitude Inline 8515 for Base, Monitor and Difference Volume

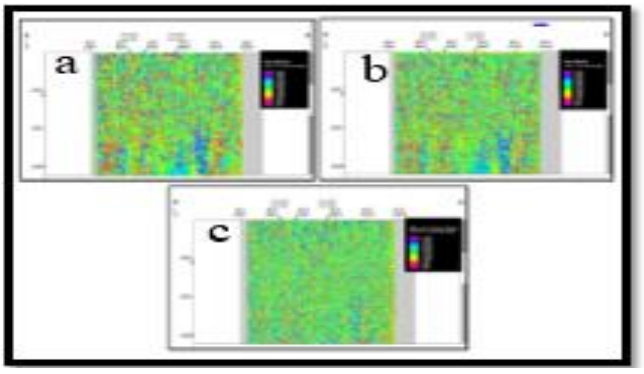

Figure 15. Azimuth Inline 8515 for Base, Monitor and Difference Volume

4.4. Fault and Horizon Interpretation

The results for the interpreted faults in Fuba field are presented in Figure 6 shows both synthetic and antithetic faults interpreted along seismic inlines. Faults are more visible along the inline direction because this direction reveals the true dip position of geologic structures. The variance time slice was used to validate the interpreted faults as shown in figure 7. The areas in black circles indicate the 4D response. All interpreted faults are normal synthetic and antithetic faults. A total of thirty-six faults were interpreted across the entire base seismic data while forty faults were interpreted across the entire monitor seismic data. Of the interpreted faults, only F1 (synthetic fault) and F16 (antithetic fault) faults are regional, running from the top to bottom across the field. Hence, these faults play significant roles in trap formation at the upper, middle and lower sections of the field. In Fuba Field, the lengths, dips and orientations of faults are not equal in both base and monitor seismic sections suggestive of fault reactivation from hydrocarbon production. The results for the interpreted seismic horizons (Horizons A and I) are also presented in Figure 6. On these horizons, the fault polygons were generated and eliminated. The horizons were used as inputs for the generation of reservoir time surfaces.

4.5. Depth Surfaces

The result of depth conversion residual analysis is presented in Table 1. The depth residual is the difference between the depth values of the well top from each well and the depth value from the depth converted reservoir surfaces. The depth residual analysis revealed that surfaces converted using the linear velocity function had the largest residuals ranging from -31.60 to +61.67 and from -50.58 to +40.84ft in reservoir A and reservoir I respectively. This is closely followed by the residual values obtained with the 2nd order polynomial function. The third order polynomial function shows the least residuals, ranging from -6.69 to +6.61 ft in reservoir A, and -9.48 to +8.42ft respectively. The negative depth residual indicates that the depth conversion process displaces the reservoir to a greater depth than where it occurs in the subsurface, while a positive depth residual signifies that the depth converted result has placed the reservoir at a shallower depth (Ogbamikhumi and Aderibigbe, 2019). The resultant depth residual values generated using the various velocity models (linear, 2nd and 3rd order polynomials) were compared in order to select the most suitable velocity model for depth conversion of the reservoir surfaces. Figure 8 shows the 3rd order polynomial velocity model which was selected and used as most suitable velocity model for converting A and I reservoirs from time to depth because it has the least residuals. The depth converted reservoir A and I surfaces are presented in Figures 9 and 10 for the third order polynomial velocity function. The depth structure maps reveal that the reservoirs are anticlinal and fault supported. Reservoir A is found at a shallower depth from 6500 to 7500 ft while reservoir I is found at a deeper depth ranging from 11500 to 13000ft respectively. The depth residuals recorded from the various well locations were used to generate depth residual maps which are presented in Figures 11 and 12 respectively. The depth residual maps revealed that higher residuals on reservoir A and I surfaces are associated with the eastern and western regions which are areas not penetrated by any well.

4.6. Variance Attribute

Figure 13 shows the computed variance attributes of the seismic section. The variance values range from 0.0 to 1.0. Values of variance equal to 1 represent discontinuities while a continuous seismic event is represented by the value

of 0. The high values are denoted with red to yellow colorations. There are more discontinuities in figure 13c which implies that there are more cracks in the field of study due to production.

Concerning the variance map, the areas dotted with blue, green, orange and pink colored lines signify values that correspond to the location of the discontinuity. The discontinuities may be interpreted as faults and boundaries as shown by the lines drawn on the variance attribute map. The variance edge enhanced the faults or sedimentological bodies within the seismic data volume. Furthermore, several bright spots are also delineated (in black circles and black ovals) which indicate high reflectivity sediments compared to their surroundings. These bright spots are an indication that a potential hydrocarbon trap might exist in the area. The variance attribute is edge imaging and detection techniques. It is used for imaging discontinuity related to faulting or stratigraphy in seismic data. Variance attribute is proven to help in imaging of channels, fault zones, fractures, unconformities and the major sequence boundaries. The darkest regions in the seismic section, which make vertical strips, may be interpreted as faults or fractures. The zones with low variance values are due to similar seismic traces. Areas with red patches represent lineaments/discontinuities while grey areas represent the structural framework of the field.

4.7. Dip Magnitude and Azimuth

Figures 14 and 15 show the dip and azimuth of the faults for the base, monitor and difference volume. The dip magnitude values range from 0 to 90 degrees while the azimuth values range from 0 to 360 degrees. On Figure 14, the green colors represent areas of greater dip, while the red colors represent areas of shallower dip. On Figure 15, the blue and orange colors represent opposite dip directions.

The dip and azimuth of the faults are not equal as indicated by the difference volume (Figures 14c and 15c). This indicates that there is fault re-activation in Fuba field due to production.

Table 1. Depth Residual between Well Tops and Resultant Depth Surfaces

Reservoir/ Well	**Well Top (ft)**	**Depth Surface (ft)**	**Difference (ft)**	**Depth Surface (ft)**	**Difference (ft)**	**Depth Surface (ft)**	**Difference (ft)**
		Linear Velocity Function		***2nd Order Polynomial***		***3rd Order Polynomial***	
Reservoir A Well-1	-7054.07	-7079.08	25.01	-7032.58	-21.49	-7053.13	-0.95
Well-2	Missing	Missing	Missing	Missing	Missing	Missing	Missing
Well-3	-6877.06	-6849.08	-27.98	-6886.40	9.34	-6880.86	3.80
Well-4	-6977.93	-7039.60	61.67	-7004.73	26.80	-6971.24	-6.69
Well-5	-6905.39	-6873.79	-31.60	-6859.58	-45.81	-6900.65	-4.74
Well-6	-7065.18	-7105.10	39.92	-7028.91	-36.27	-7070.87	5.69
Well-7	-6846.24	-6877.44	31.20	-6854.65	8.41	-6852.85	6.61

Reservoir I Well-1	-11690.91	-11720.12	29.21	-11674.22	-16.69	-11690.91	0.00
Well-2	-11823.41	-11780.54	-42.87	-11807.54	-15.87	-11823.41	0.00
Well-3	-11650.06	-11684.44	34.38	-11666.36	16.30	-11656.67	6.61
Well-4	-11887.08	-11845.26	-41.82	-11912.42	25.34	-11877.60	-9.48
Well-5	-11599.86	-11549.01	-50.85	-11581.29	-18.57	-11595.11	-4.75
Well-6	-11569.00	-11534.94	-34.06	-11586.60	17.60	-11564.27	-4.73
Well-7	-11551.91	-11592.75	40.84	-11534.64	-17.27	-11560.33	8.42

5.0. Conclusion

Production decline of 1192.21bbl/day resulted from pressure decline of 95.50bar/year or 0.062psi/year. Most of the data points were not repeatable as evidenced in the computed Normalized root mean square (NRMS) of 0.38 meaning that on 62.0% of Base and Monitor data points were coincident. A total of nine sand bodies (A, B, C, D, E, F, G, H and I) were identified and correlated across all seven wells in the field. Two horizons (A and I) were selected for the study. Structural interpretation of seismic data revealed that the field is highly faulted with synthetic and antithetic faults which are in line with faults trends identified in the Niger Delta. Fault and horizon interpretation revealed that closures found are collapsed crestal structures bounded by two major faults. The depth structure maps reveal anticlinal faults. Reservoirs are found at a shallower depth from 6500 to 7500 ft and at a deeper depth ranging from 11500 to 13000ft. The synthetic and antithetic faults act as good traps for the hydrocarbon accumulation in the study area. The variance edge enhanced the faults or sedimentological bodies within the seismic data volume. There are more discontinuities in the difference volume variance edge which implies that there are more cracks in the field of study due to production. The lengths, dips and orientations of the faults and horizons, in the base and monitor stacks, are not equal indicative of faults reactivation that could have resulted from hydrocarbon production. In reservoirs, hydrocarbons were encountered by all seven wells drilled in the field. Deterministic hydrocarbon volume estimation of the area of study indicates large quantities of hydrocarbon at the intervals where these structures were mapped. Within the limits of the available data, it is recommended that further studies should include integration of stratigraphic data of all the wells. This will provide more reliable data for interpretation of the depositional environments. Also, further studies are required to confirm if these faults are sealing or leaking.

Declarations

Source of Funding

This study did not receive any grant from funding agencies in the public or not-for-profit sectors.

Competing Interests Statement

The author has declared no competing interests.

Consent for Publication

The author declares that she consented to the publication of this study.

Acknowledgements

The author is grateful to Shell Petroleum Development Company of Nigeria (SPDC), Port Harcourt Nigeria for the release of the academic data for the purpose of this study.

References

[1] Stammeijer, J.G.F. & Hatchell, P.J. (2014). Standards in 4D Feasibility and interpretation. The Leading Edge, 33, Pages 134–140.

[2] Landrø, M. (2001). Discrimination Between Pressure and Fluid Saturation Changes from Time-lapse Seismic Data: Geophysics, 66(3): 836–844.

[3] Trani, M., Arts, R., Leeuwenburgh, O. & Brouwer, J. (2011). Estimation of Changes in Saturation and Pressure from 4D Seismic AVO and Time-shift Analysis. Geophysics, 76: 1–17.

[4] MacBeth, C., Mangriotis, M.D. & Amini, H. (2019). Post-stack 4D Seismic Time-shifts: Interpretation and Evaluation. Geophysical Prospecting, 67: 3–31.

[5] Prioul, R., Bakulin, A. & Bakulin, V. (2004). Nonlinear rock physics model for estimation of 3D subsurface stress in anisotropic formations: Theory and laboratory verification. Geophysics, 69: 415–425.

[6] Fuck, R.F., Tsvankin, I. & Bakulin, A. (2011). Influence of background heterogeneity on traveltime shifts for 15 compacting reservoirs. Geophysical Prospecting, 59: 78–89.

[7] Alsos, T., Eide, A., Astratti, D., Pickering,S., Benabentos, M., Dutta, N., Mallick, S., Schultz, G., Den Boer, L., Livingston, M., Nickel, M., Sonneland, L., Schlaf, J., Schoepfer, P., Sigimondi, M., Soldo, J.C. & Stronen, L.K, (2002). Seismic Applications throughout the Life of a Reservoir. Oilfield Review, 14: 48–65.

[8] Zoback, M.D. & Zinke J.C. (2002). Production –Induced Normal Faulting in the Valhall and Ekofisk Oil Fields. Pure and Applied Geophysics, 159: 403–420.

[9] Aniwetalu, E.U., Anakwuba, E.K., Ilechukwu, J.N. & Aikegwuonu, O.N. (2017). Application of Time Lapse (4D) Seismic Data in Locating Hydrocarbon Prospects in Udam Field, Onshore Niger Delta, Nigeria. Petroleum and Coal, 59(5): 715–722.

[10] Uko, E.D., Famuyibo, D.A. & Okiongbo, K. (2018). Estimation of Land Surface Subsidence Induced by Hydrocarbon Production in the Niger Delta, Nigeria, using Time-Lapse Orthometric Leveling Data. Mediterranean Journal of Basic and Applied Sciences, 2(3): 1–18.

[11] Igwenagu C.L., Uko E.D., Tamunobereton-Ari I. & Amakiri A.R.C (2021). The Subsurface Structures in KOCR Field in the Niger Delta, Nigeria, Using 3d Seismic Timelapse Data. Geological Behavior, 5(1): 7–12.

[12] Minkoff, S.E., Stone, C.M., Bryant, S. and Peszynska, M. (2004). Coupled geomechanics and flow simulation for time-lapse seismic modelling. Geophysics, 69: 200–211.

[13] Herwanger, J.V. and Horne, S.A. (2009). Linking Reservoir Geomechanics and Time-Lapse Seismics: Predicting Anisotropic Velocity Changes and Seismic Attributes. Geophysics, 74 (4): 13–33.

[14] Whiteman, A. (1982). Nigeria: Its Petroleum Ecology Resources and Potential. London, Graham and Trotman.

[15] Adegoke, O.S., Oyebamiji, A.S., Edet, J.J, Osterloff, P.L. & Ulu, O.K (2017). Cenozoic Foraminifera and Calcareous Nannofossil Biostratigraphy of the Niger Delta. Elsevier, Cathleen Sether, United States.

[16] Short, K.C. & Stable A.J. (1967). Outline of Geology of Niger Delta. Bulletin of America Association of Petroleum Geologists, 51(5): 761–779.

[17] Horsfall, O.I., Uko, E.D., Tamunoberetonari I. & Omubo-Pepple, V.B. (2017). Rock-Physics and Seismic-Inversion Based Reservoir Characterization of AKOS Field, Coastal Swamp Depobelt, Niger Delta, Nigeria. IOSR Journal of Applied Geology and Geophysics, 5(4): 59–67.

[18] Ochoma, U., Uko E.D. & Horsfall, O.I. (2020). Deterministic Hydrocarbon Volume Estimation of the Onshore Fuba Field, Niger Delta, Nigeria. IOSR Journal of Applied Geology and Geophysics, 8(1): 34–40.

[19] Vedanti, N., Pathak, A., Srivastava, R.P. and Dimri, V.P. (2009). Time Lapse (4D) Seismic: Some Case Studies. e-Journal Earth Science India, 2(4): 230–248.

[20] Varela, O.J., Torres-verdin, C., Sen, M.K. and Roy, I.G. (2006). Using Time-lapse Seismic Amplitude Data to Detect Variations of Pore Pressure and Fluid Saturation Due to Oil Displacement by Water: A Numerical Study Based on One-Dimensional Prestack Inversion. Journal of Geophysics and Engineering, 3: 177–193.

[21] Kragh, E. & Christie, P. (2002). Seismic Repeatability, Normalized Rms, and Predictability. The Leading Edge, 21(7): 640–647.

[22] Johnston, D.H. (2013). Practical Applications of Time-lapse Seismic Data. SEG Distinguished Instructor Series No. 16, SEG.

[23] Pigott. J.D., Kang, M.I.H. & Han, H.C. (2013). First Order Seismic Attributes for Clastic Seismic Facies Interpretation: Examples from the East China Sea. Journal of Asian Earth Science, 66: 34–54.

[24] Ogbamikhumi, A. & Aderibigbe, T.O. (2019). Velocity Modelling and Depth Conversion Uncertainty Analysis of Onshore Reservoirs in the Niger Delta Basin. Journal of the Cameroon Academy of Sciences, 14(3): 239–247.